JOURNAL OF GEOPHYSICAL RESEARCH, VOL. 106, NO. D24, PAGES 34,021–34,034, DECEMBER 27, 2001

Observation and analysis of ice flow in the largest Greenland ice stream

Ian Joughin,[1] Mark Fahnestock,[2] Doug MacAyeal,[3] Jonathan L. Bamber,[4] and Prasad Gogineni[5]

Abstract. We have applied satellite radar interferometry methods to map the velocity field of the recently discovered Northeast Greenland Ice Stream. We have used these data in conjunction with ice thickness and accumulation data to determine that the ice stream is in balance within the measurement errors. We used control methods to invert a finite element model of ice sheet flow constrained by the data to infer the ice stream's basal shear stress distribution. Our results reveal that flow in a section of the downstream end has much in common with the streaming flow of the Ross Ice Streams of West Antarctica (e.g., a weak bed and fast flow in the presence of low driving stresses). For several hundred kilometers along the middle of the ice stream, the basal shear stress balances the driving stress. In the upstream area, where the ice stream is first visible in the velocity data, the bed appears to be weak, which may contribute to the initiation of the ice stream.

1. Introduction

Only recently discovered through the analysis of synthetic aperture radar (SAR) imagery [*Fahnestock et al.*, 1993], the Northeast Greenland Ice Stream is a nearly straight feature ~700 km long with distinct margins for most of its length and a topographically undulating interior resulting from rapid ice flow over the bed topography. Given its unique geometry and dynamics, as well as its potential impact on mass balance, the Northeast Greenland Ice Stream is an important feature for glaciological study.

In the simplest model of ice sheet flow, with ice that is frozen to the bed and deforming internally in response to surface slope and thickness, the potential for a rapid change in balance due to flow instabilities is limited. If, however, one considers the rapid sliding exhibited by ice streams and outlet glaciers in Greenland and Antarctica, the potential for a rapid change in mass balance is much greater. Furthermore, the balance state of the surrounding ice sheet becomes much more difficult to assess. The enhanced flow of the Northeast Greenland Ice Stream, which extends deep within the interior of the ice sheet, represents a departure from simple sheet flow. The flow within the ice stream is governed by physical processes that are not well understood and thus are difficult to model. Thus, understanding the origins and mechanics of this and other large ice streams is critical to improving our ability to model and to predict ice sheet evolution and the associated impact on sea level.

[1]Jet Propulsion Laboratory, California Institute of Technology, Pasadena, California.
[2]Earth System Science Interdisciplinary Center, University of Maryland, College Park, Maryland.
[3]Department of Geophysical Sciences, University of Chicago, Chicago, Illinois.
[4]Centre for Remote Sensing, School of Geographical Sciences, University of Bristol, Bristol, England, United Kingdom.
[5]Radar Systems and Remote Sensing Laboratory, University of Kansas, Lawrence, Kansas.

Paper number 2001JD900087.
0148-0227/01/2001JD900087$09.00

The harsh environments and remote locations of Greenland and Antarctica have made it difficult to make glaciological measurements such as ice flow velocity and elevation. Even in areas where extensive in situ measurements have been made, there are, at best, only a few hundred velocity measurements available. This has complicated efforts both to model ice stream and glacier dynamics and to determine ice sheet mass balance.

Over the last decade, satellite remote sensing has begun to open up the ice sheets to more detailed and quantitative study. In particular, significant progress has been made in the area of satellite radar interferometry (SRI), which was first used to observe ice motion by *Goldstein et al.* [1993]. Since that time, SRI technique has evolved to the point where it is now possible to combine data from many passes to produce topography and vector velocity measurements over large areas of the ice sheets [*Joughin et al.*, 1999, 2000].

Our study of the Northeast Greenland Ice Stream makes use of a combination of remote sensing and ice sheet modeling techniques. We begin with a description of velocity and elevation maps generated from SRI data, which cover nearly the entire ice stream. In conjunction with ice thickness data collected by the University of Kansas sounder [*Gogineni et al.*, this issue] we have assessed the ice stream mass balance. Finally, we also have used the data to constrain inversions of existing models for conditions at the bed. These experiments have improved our understanding of basal processes controlling the ice stream; in addition, they have revealed the limitations of an existing model, suggesting areas for further model development. *Fahnestock et al.* [this issue] discuss the onset of rapid flow in the upper half of the ice stream, relating the measured strain rates and flow patterns to surface morphology, ice-penetrating radar measurements of bed conditions, and repeat laser altimeter measurements.

2. Ice Stream Observations

2.1. Interferometric Processing

We have processed several hundred gigabytes of SAR data from the ERS-1 and ERS-2 satellites to produce a map of

velocity on the surface of the Northeast Greenland Ice Stream (Plate 1). SAR data from many crossing descending and ascending orbits were combined to produce vector measurements on the basis of the assumption of surface parallel flow [*Joughin et al.*, 1998; *Mohr et al.*, 1998]. In a few areas where we had data from only a single track direction, we were able to derive vector measurements using a technique called "speckle tracking," which takes advantage of the ability to determine with subpixel accuracy the displacements (both across and along track) between scenes in an interferometric pair [*Michel and Rignot*, 1999; *Gray et al.*, 1998]. Further details are given by *Joughin et al.* [2000]. The resulting map is one of the largest ever made of surface deformation (of any type) at subkilometer resolution.

Accurate interferometric velocity measurements require centimeter or better accuracy for the interferometer baseline, which is the distance separating the satellite tracks on nearly repeating orbits. The orbits of the ERS-1 and ERS-2 spacecraft are not known well enough to provide sufficiently accurate baselines. As a result, points of known velocity and elevation (control points) are needed to solve for the baseline. Ideally, these control points would be acquired using repeat GPS surveys of stakes in the ice. Although some GPS measurements were collected for this map, it was not possible to acquire enough points to provide an adequate source of control for the large number of satellite tracks over this area. Instead, we opted to use balance velocities as a source of control. Balance velocities are the depth-averaged velocities necessary to maintain the steady state shape of the ice sheet and are estimated from surface slope, ice thickness, and accumulation data [*Paterson*, 1994]. We computed these values as described by *Joughin et al.* [1997] and rescaled them by a factor of 1.1 for conversion from depth-averaged to surface velocity. This conversion factor is a rough estimate and falls between the value of 1.25 for temperate ice [*Paterson*, 1994] and 1.0 for motion entirely due to sliding. Even with no sliding, the value for an ice sheet is smaller than that for temperate ice because more deformable ice is concentrated at the base of the ice sheet where temperatures are warmer than nearer the surface. Better estimates of this spatially variable conversion factor could be obtained with a thermomechanical ice sheet model [*Thomas et al.*, 1998]. The resulting improvement, however, would be small (e.g., a few percent) with respect to other sources of error.

In estimating the baselines we selected balance velocities as control points only from slow moving areas (i.e., <30 m/yr) where relative errors might be large (i.e., 25–50%) but absolute errors would remain small (i.e., <10 m/yr). We used a least squares fit to a large number of control points, which helps reduce the random (uncorrelated) component of the error in the control points. We did not use the GPS measurements in the baseline solutions, saving them, instead, for validation. We found that the 12 GPS measurements that lie within the area covered by the map agree with the interferometric velocities to within 5 m/yr [*Joughin et al.*, 2000].

Interferometry can also be used to estimate surface topography. This requires two sets of interferograms in order to separate the effects of motion and topography. Unfortunately, the data contained several long-wavelength artifacts that reduced the accuracy of the digital elevation model (DEM) below that of existing lower-resolution data sets. As a result, we retained only the short-scale topographic information from the interferometry and blended it with existing satellite altimeter data [*Bamber et al.*, 2001] to create a DEM with improved resolution (better than 500 m) [*Joughin et al.*, 2000]. A shaded surface representation of this DEM is shown in Figure 1. The areas where we could improve the DEM correspond roughly with the areas where velocity data are shown in Plate 1. The improvement in resolution is evident in areas where the DEM fades from interferometry blended with altimetry data to only altimetry data.

2.2. Airborne Data Sets

As part of the Program for Arctic Regional Climate Assessment (PARCA) effort, ice thickness profiles were collected from an aircraft using the University of Kansas Coherent Radar Depth Sounder (CoRDS) [*Gogineni et al.*, this issue]. Accompanying surface elevation profiles were collected by the NASA Airborne Topographic Mapper (ATM) laser altimeter [*Krabill et al.*, 2000]. Several of these profiles cross the ice stream at the locations shown with yellow lines in Plate 1. The three profiles that run longitudinally down the ice stream are labeled L1–L3, while the eight transverse profiles are labeled T1–T8. The bed and surface elevation data along with the flow speeds from the longitudinal profiles (L1–L3) are shown in Figure 2, while the corresponding data from the transverse profiles (T1–T8) are shown in Figure 3.

Figures 2 and 3 show the CoRDS profiles at the full resolution but make it difficult to visualize the overall regional bed topography. The CoRDS ice thickness data collected between 1993 and 1999 were combined with data collected by the Technical University of Denmark in the 1970s to produce a new ice thickness grid for Greenland [*Bamber et al.*, this issue]. Crossover analysis was used to assess the relative accuracy of the two data sets, and they were weighted accordingly and interpolated onto a regular grid using an optimal interpolation procedure. A high-resolution land-ice mask was used to help constrain the interpolation of the ice thickness near the ice sheet margins where, in the past, the relative errors have been largest. The ice thickness grid was combined with a new digital elevation model of the ice sheet and surrounding rock outcrops to produce a new bed elevation data set for the whole of Greenland. The accuracy of the bed elevation model ranges from 10 to ~200 m, depending on the local data source and its proximity to a grid point.

Plate 2 shows the bed topography in the vicinity of the ice stream with color-coded elevations. Flow speed contours have been plotted over the DEM to show the location of the ice stream. The boundaries of the drainage that feeds Zachariæ Isstrøm, Nioghalvfjerdsfjorden, and Storstrømmen are shown with thick black lines. At several elevation contours within the basin (orange lines), we have plotted flow lines extending upstream from where the contour intersects the margins of the ice stream to show the origin of ice entering the stream at various points along its length.

2.3. Discussion

The velocity map (Plate 1) reveals a pattern of organized flow extending deep into the interior of the ice sheet. The ice stream first manifests itself as a roughly 15-km-wide area of enhanced flow starting within ~100 km of the ice divide. While the speed is initially only ~10 m/yr greater than that of the surrounding ice, the enhanced flow is delineated by well-defined shear margins (see also T1 and T2 in Figure 3). Downstream, a tributary of slightly enhanced flow merges with the ice stream. This tributary, which is barely visible in Plate 1 but

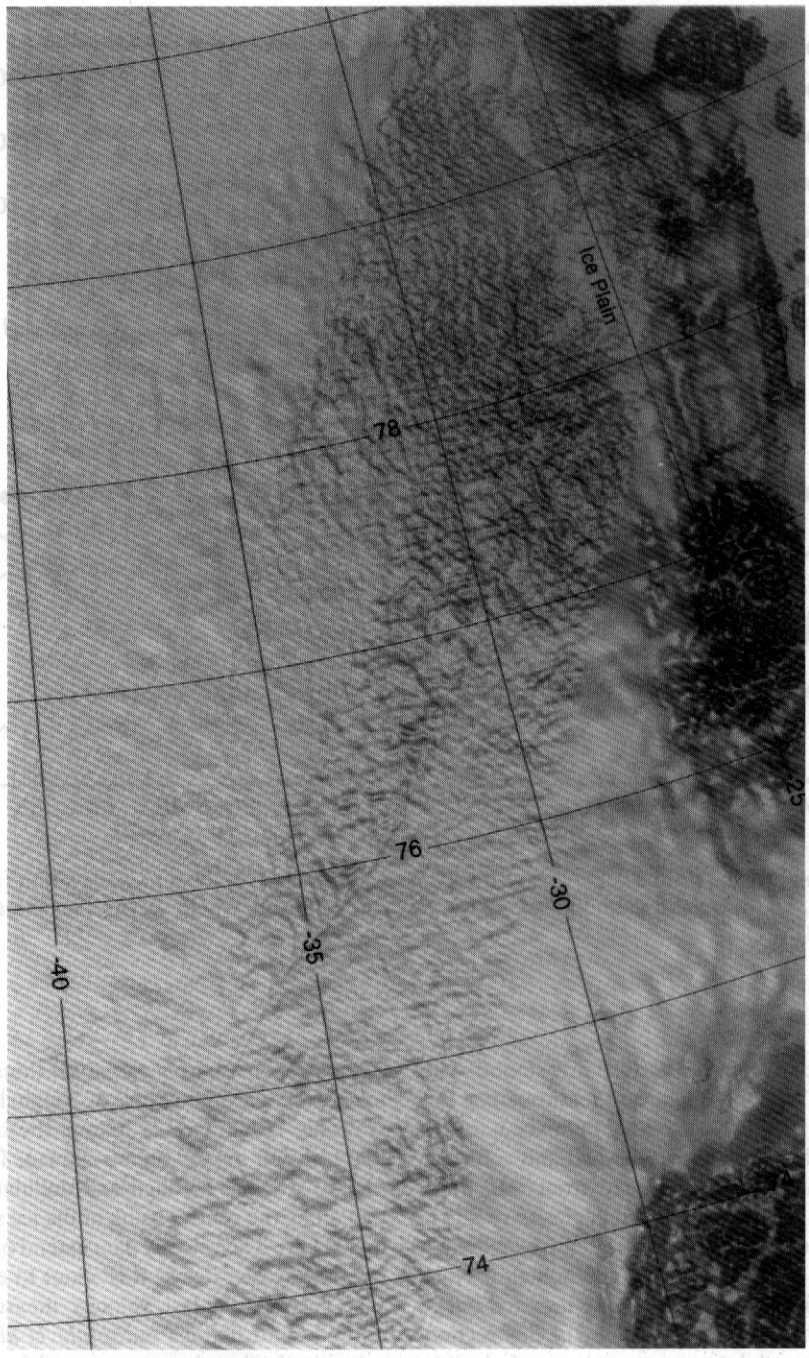

Figure 1. Shaded surface of digital elevation model (DEM) for the Northeast Greenland Ice Stream. The vantage point and light source are directly overhead. Where SAR data were available on the ice sheet, the DEM is a blend of interferometric and radar altimetry data. In other ice-covered areas the data are primarily from radar altimetry. The ice-free coastal data were photogrammetrically derived [*Ekholm*, 1996].

is apparent in profiles T1 and T2 (Figure 3), is much broader and, in contrast to the first tributary, lacks well-defined shear margins. Downstream from the merger with the tributary, the width of the ice stream increases to ~60 km, with flow speeds of 50–60 m/yr. At this point the ice stream is visible in the DEM as an area of rougher surface topography. At ~300 km downstream (T5 in Figure 3) the flow begins to concentrate on the southeastern side of the ice stream. This narrowing of the main trunk results in an increase in speed to ~125 m/yr. At nearly 540 km along profile L1 (Figure 2), the surface of the ice flattens out, forming a large ice plain, which can be seen in Figure 1 as the smoother surface just downstream of a broad band of rougher topography. We use the term ice plain here to describe the nearly flat surface on the ice sheet. This is not meant to imply any similarity to the dynamics of the ice plain found on Ice Stream B, West Antarctica. Just upstream of the ice plain, the flow divides with a southern branch feeding Storstrømmen and a northern branch flowing through the ice plain to feed the outlet glaciers of Zachariæ Isstrøm and Nioghalvfjerdsfjorden.

The longest airborne profile, L1 (Figure 2), runs nearly the full length of the ice stream. Over the uppermost section (0–

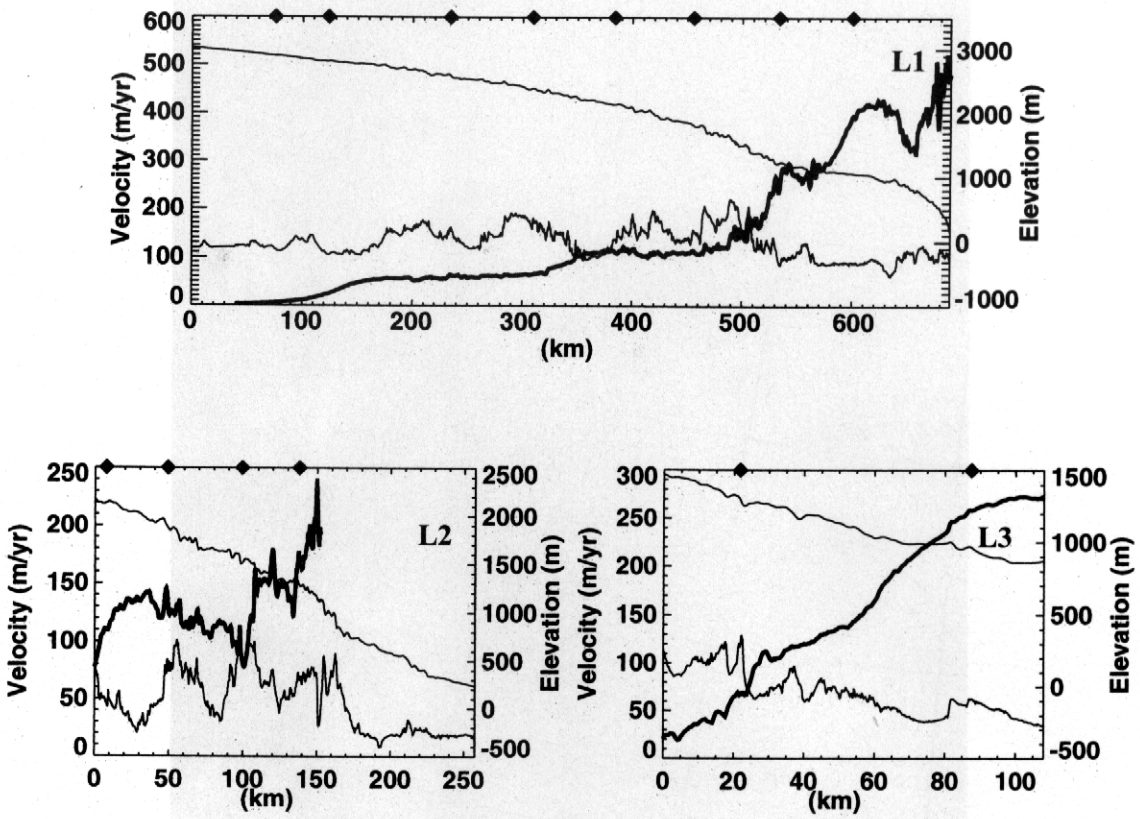

Figure 2. Longitudinal profiles of velocity (thick curve) and surface and bedrock elevation (thin curves) for profiles L1, L2, and L3. Solid diamonds along the top x axis indicate where the profiles intersect transverse profiles (see Plate 1).

150 km) the profile indicates that the bed is fairly smooth with little topographic relief. The only significant feature along this sector of the profile is a roughly 30-km-long bump centered at 100 km that rises roughly 300 m above the bed and coincides with the beginning of an increase in speed from ~10 to 60 m/yr. At ~150 km along the profile the bed begins to roughen, with large undulations of 500–600 m in height over length scales of nearly 100 km. Some of these large undulations may be the result of the profile repeatedly crossing into and out of a subglacial channel, which is discussed later in this section. Superimposed on these undulations is a pattern of shorter-wavelength variations (e.g., 10 km) with amplitudes of ~100–200 m. The increased roughness of the bed and the higher flow speeds yield a bumpier surface on the ice stream (see Figure 1). In particular, in the region between 400 and 500 km, there are peaks and troughs in the surface topography of well over 100 m, which is extreme topography for the surface of an ice sheet. Speeds over this undulating region (150–500 km) increase gradually from ~60 to 100 m/yr.

The surface slope increases significantly over the interval from 500–530 km as the ice flows over a large bedrock obstacle. Beyond this obstacle the speed increases abruptly from roughly 100 to 400 m/yr as the bed begins to smooth out and remains nearly flat at ~300 m below sea level from ~530 to 630 km. This coincides with the ice plain (see also Figure 1), which represents a significant departure from a typical parabolic ice sheet profile. After a small dip in the bed (640 km) the slope steepens sharply as the ice thins and accelerates rapidly toward the grounding line of Nioghalvfjerdsfjorden.

Profile L2 (Figure 2) follows the branch of the ice stream that forks off to feed Storstrømmen. The bed along this profile (0–150 km) has a rough and undulating character similar to that along the central trunk of the ice stream (e.g., L1 from 150 to 500 km). The velocity data extend only up to the point where the flow accelerates as it is about to enter the fjord (150 km). Just beyond the last velocity measurement the bed drops abruptly and flattens out. *Mohr et al.* [1998] have computed velocities farther downstream and found that the ice begins to decelerate to nearly a complete stop at the grounding line, which is a situation that has been present since a surge in the late 1980s and early 1990s [*Reeh et al.*, 1994].

The last longitudinal profile, L3, follows the main tributary of Nioghalvfjerdsfjorden, which is distinct from the ice stream. Unlike the ice stream, which begins well inland, enhanced flow along this tributary begins much nearer the coast at ~100 km from its merger with the ice stream. At ~25 km along the profile, there is a drop of ~500 m in the bed, with the velocity increasing steadily over the next 75 km to ~270 m/yr.

The first two transverse profiles, T1 and T2 (Figure 3), cross the narrow upper part of the stream (see Plate 1). The broad tributary flow is visible just to the right of the more distinct ice stream flow in both profiles. The raised feature in the bed that was visible in the longitudinal profile L1 (at 100 km) is seen in profile T1. Its width corresponds well with that of the ice

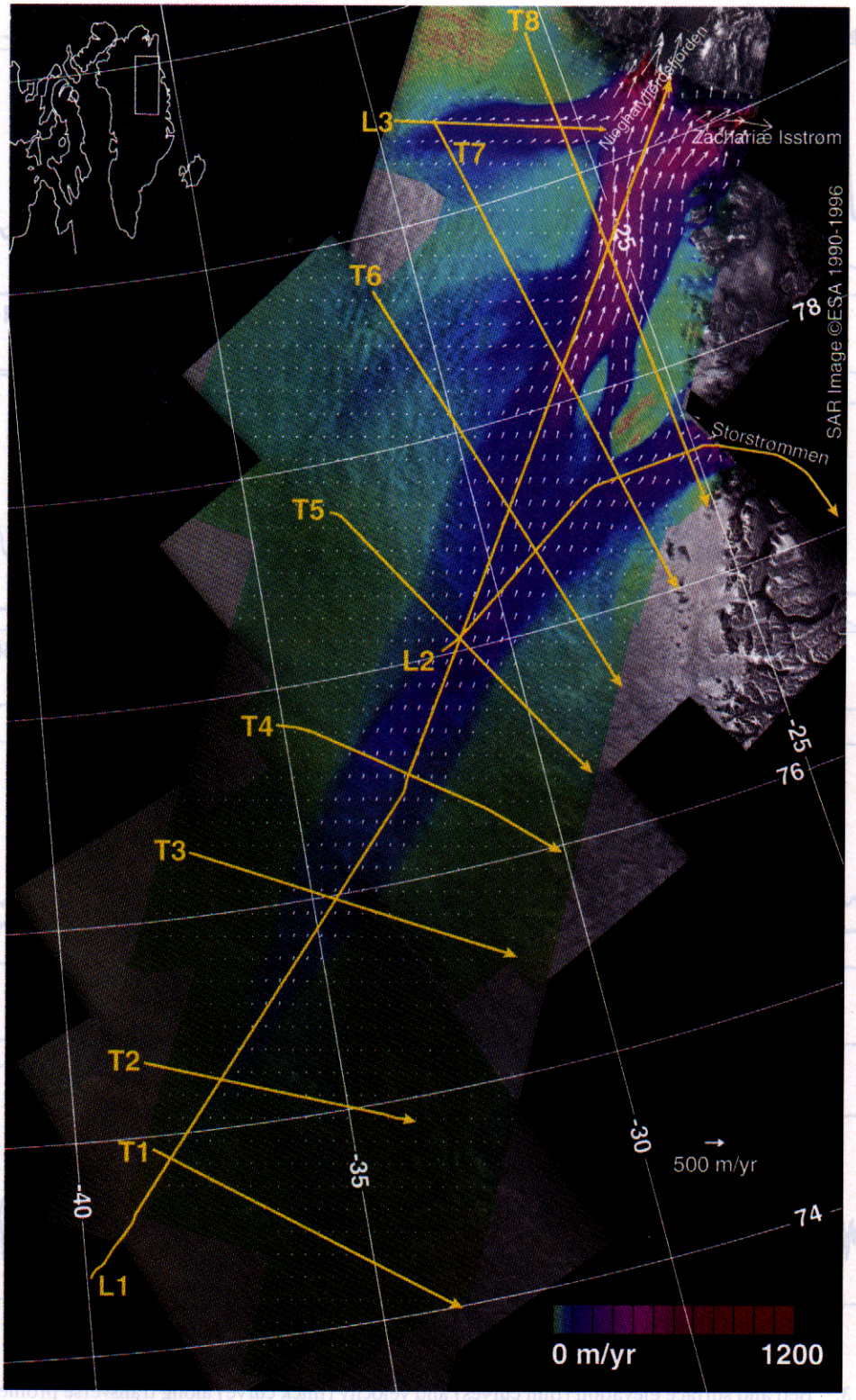

Plate 1. Velocity of the Northeast Greenland Ice Stream. Speed is displayed as color over synthetic aperture radar (SAR) imagery. Subsampled velocity vectors are shown with white arrows. Yellow lines (with arrows to indicate plot direction) show the location of profiles plotted in subsequent figures.

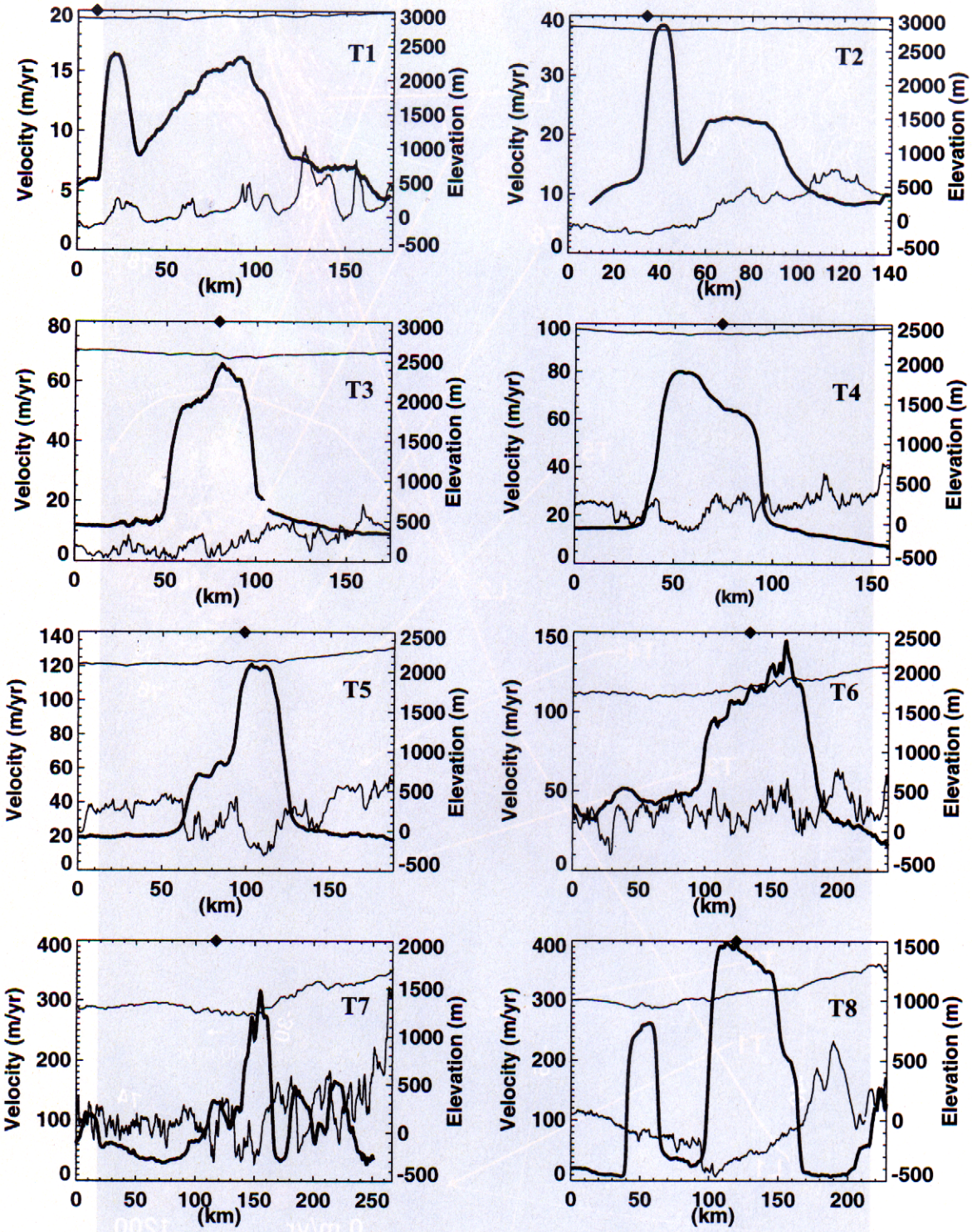

Figure 3. Bed and surface elevation (thin curves) and velocity (thick curve) along transverse profiles T1–T8. Solid diamonds along the top x axis indicate where the profiles intersect the longitudinal profile, L1 (see Plate 1).

stream, suggesting that it may play some role in the enhanced flow of the ice stream at this point. Downstream at profile T2, the ice stream maintains its narrow width at a speed of nearly 40 m/yr, with little corresponding topographic expression at the bed.

Profiles T3–T6 cross the main trunk of the ice stream before the flow divides farther downstream. At profile T3 the ice stream has widened out to roughly 50 km with speeds just over 60 m/yr. Despite the well-defined shear margins, there is little evidence of any kind of channel in the bed topography. At profile T4 the speed has increased to 80 m/yr with the peak in velocity now at the left half of the profile coincident with what

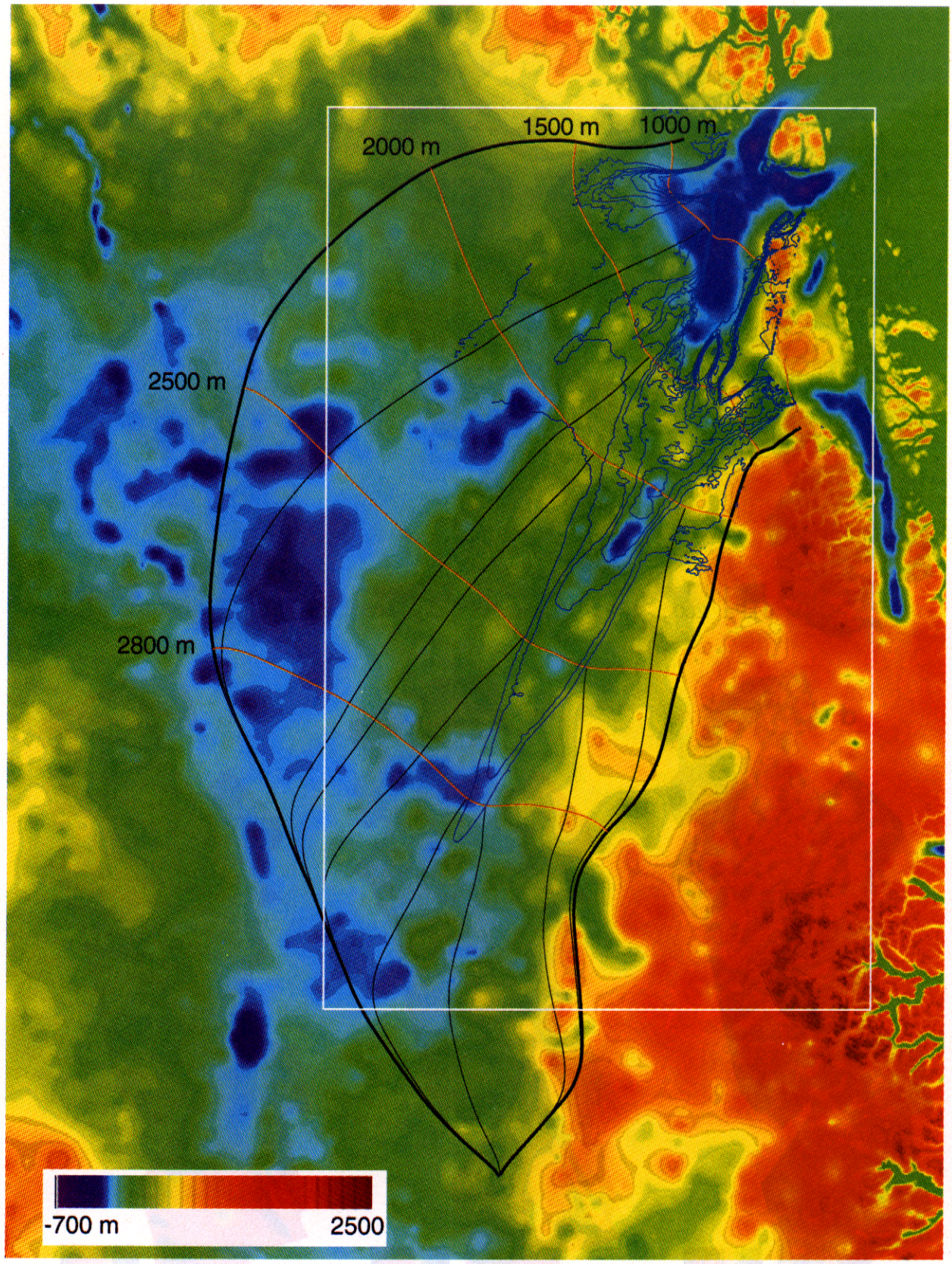

Plate 2. Ice stream speed contours, flow lines, and elevation contours plotted over bed topography (color coded). The location of the ice stream with respect to the topography is shown with speed contours (blue lines) from 25 to 200 m/yr. The outline of the drainage basin is shown with thick black curves. Orange lines are used for the 2800-, 2500-, 2000-, 1500-, and 1000-m surface elevation contours within the basin. Flow lines (thin black lines) are shown extending upstream from where the ice stream margins intersect each elevation contour. The white box indicates the area shown in Plate 1 and Figure 1.

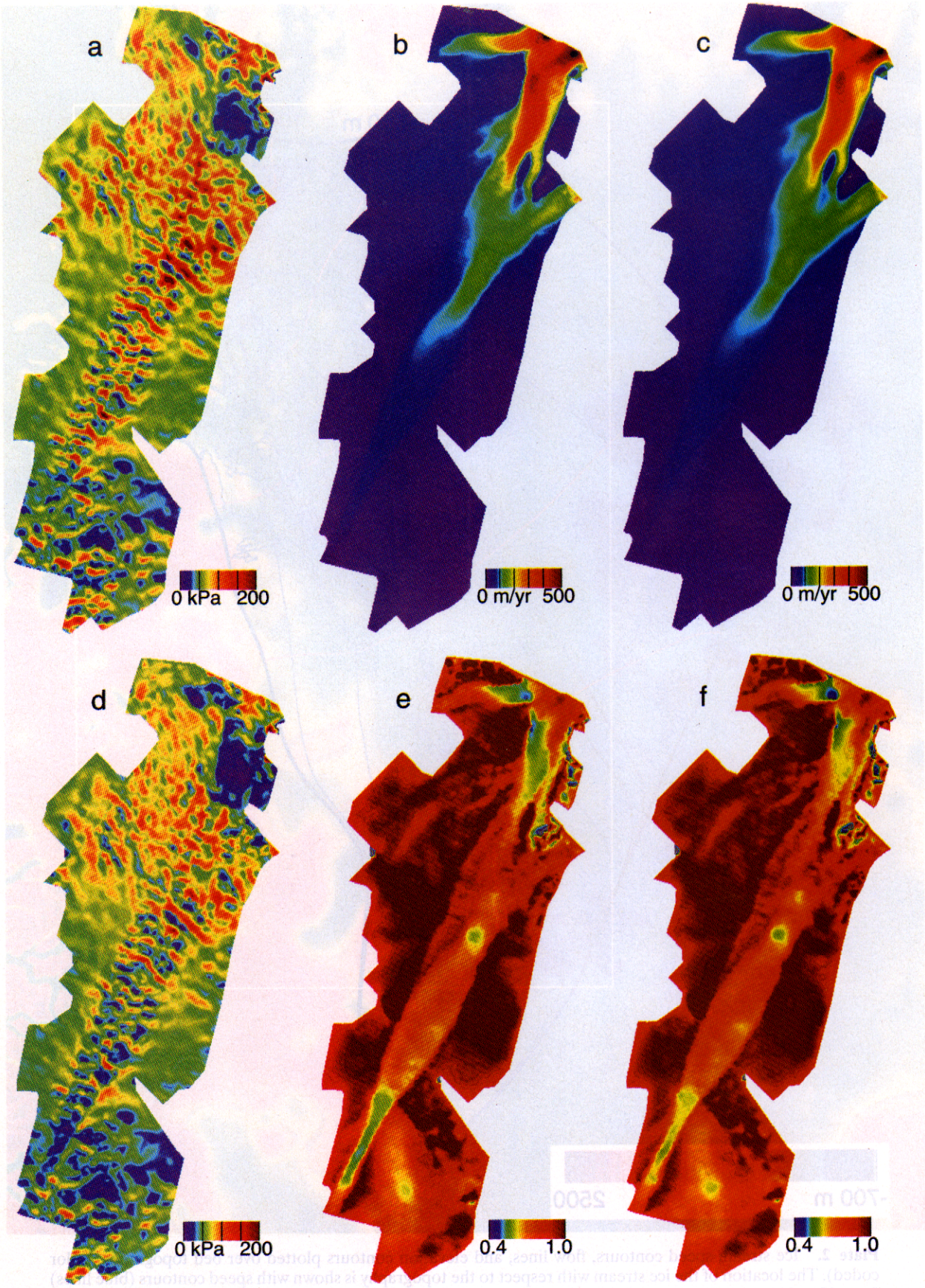

Plate 3. Inputs to and results from model inversions, showing (a) driving stress, (b) observed speed, (c) speed from inversion of cold model, (d) inferred basal shear stress for cold model, (e) ratio of basal shear stress to driving stress for cold model, and (f) ratio of basal shear stress to driving stress for warm model. The area where data are plotted corresponds to the area where we have velocity data (see Plate 1).

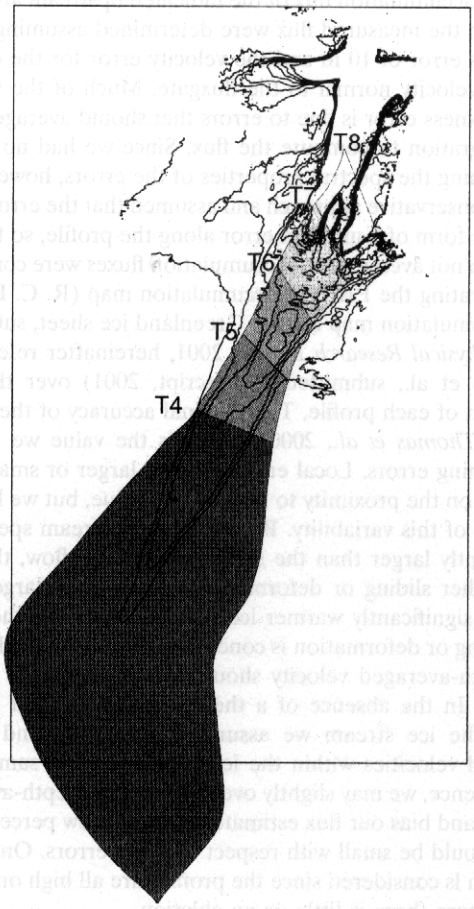

Figure 4. Regions, gates, and bounding flow lines used in mass balance estimates. The box indicates the area shown in Plate 1 and Figure 1.

appears to be a channel ~400 m deep. Flow along this "channel," however, is only ~20 m/yr faster than flow over the other half of the ice stream where there are no channel-like features. At profile T5 the flow is concentrated along the right half of the stream, with the bed topography suggesting a prominent channel. At profile T6 the bed roughens with peaks in the bed topography that spatially correspond with "spikes" in the velocity field. These velocity spikes likely occur as the ice must speed up to maintain ice flux continuity as the ice thins over bedrock highs. The flow at this point is more evenly distributed across the width of the ice stream, and there are no easily distinguished channel-like features visible in the bed.

Profile T7 spans the area upstream of the ice plain, which corresponds to the very bumpy area visible in Figure 1. There

Table 1. Measured Fluxes, Accumulation Fluxes, and Areas for Regions and Profiles Shown in Figure 4[a]

Profile	Area, km^2	Measured Flux, km^3 WE	Accumulation Flux, km^3/yr WE
T4	71,765	8.5 ± 0.8	10.2 ± 1.0
T5	76,861	9.2 ± 0.6	10.9 ± 1.1
T6	80,654	9.9 ± 0.5	11.4 ± 1.1
T7	85,023	9.2 ± 0.5	11.9 ± 1.2
T8	88,864	10.6 ± 0.6	12.4 ± 1.2

[a]All flux values are water equivalent (WE).

Table 2. Flux Differences Between Pairs of Gates and Estimated Rate of Elevation Change[a]

Profiles	Measured Flux Difference, km^3/yr WE	Accumulation Flux Difference, km^3/yr WE	dh/dt, m/yr
T5-T4	0.7 ± 1.1	0.7 ± 0.07	0.00 ± 0.19
T6-T5	0.8 ± 0.8	0.5 ± 0.05	−0.06 ± 0.20
T7-T6	−0.7 ± 0.7	0.6 ± 0.06	0.27 ± 0.16
T8-T7	1.5 ± 0.8	0.5 ± 0.05	−0.24 ± 0.19
T8-T4	2.1 ± 1.1	2.1 ± 0.21	0.00 ± 0.06

[a]Estimated rate of elevation change is dh/dt. Note that the errors for the differences in fluxes are independent and are combined as independent random variables. The flux differences are equivalent to the accumulation for the area between profiles, which have error estimates of 10%.

are several peaks and valleys in the bed profiles with relief of >500 m. While it is not clear how much of a channel exists at this point, it is clear that the slow moving spot in the middle of the ice stream is where a bedrock obstruction is large enough to force flow primarily around rather than over it. At the far right of profile T7 the bed rises nearly to the surface in an area near several nunataks visible in the SAR imagery.

Farther downstream at profile T8, the bed is much smoother in the region under the ice plain. The velocity is less variable and peaks at 400 m/yr for the northern branch of the ice stream that discharges through Zachariæ Isstrøm and Nioghalvfjerdsfjorden, reflecting the transition from a rough to smooth bed. In contrast, the bed remains rough along the section of profile T8 that discharges through Storstrømmen (200–250 km).

The bed DEM in Plate 2 indicates that the upper reaches of the ice stream and much of the area along the western part of the drainage basin fall within an area slightly below sea level. While much of this area is relatively flat, there are several small peaks that lie near the beginning of the ice stream. Two of these peaks are just upstream of the head of the ice stream (i.e., the 25 m/yr contour).

The eastern boundary of the drainage basin follows the edge of the large highland area to the east of the ice stream (e.g., the largely red area). The edge of this raised area coincides with a large bend in the drainage boundary. This bend and associated basal topography likely contribute to the initiation of the ice stream. If the bed were flat, the flow lines would diverge as the ice moves toward the coast. Instead, by having to flow around the raised area the flow lines at 2800 m converge sharply, leading to an increase in flow speed at the upper end of the ice stream. In contrast, the western part of the basin is largely drained by sheet flow, where the flow lines are divergent or weakly convergent with strong convergence only near the coast. Although the bed seems to force a region of strong convergence to give rise to the ice stream, it is not clear why the ice stream should begin as such a sharply defined feature.

Downstream of the 2800-m contour the ice stream flows through an area that is raised ~300–400 m above the low-lying area to the west (e.g., the blue area in Plate 2). As the CoRDS profiles (Figures 2 and 3) indicate, the bed over which the ice stream flows is relatively rough. Along the middle portion of the ice stream the channel that was visible in the transverse profiles is evident in the bed DEM with a corresponding influence on the pattern of flow within the stream, although the channel is significantly narrower than the width of the ice stream. The channel is only well defined over a few hundred

kilometers of the total length of the ice stream, indicating that the linear geometry of the ice stream cannot be fully explained by the presence of a subglacial channel.

At 1500 m the ice flux from ~55% of the upstream drainage area has been incorporated into the ice stream. The remainder of the basin is drained largely by two distinct flow units to the west, which merge with the ice stream farther downstream. The first of these, which comprises ~20% of the basin, follows a predominantly subsea-level area with its eastern boundary skirting the raised area over which the ice stream flows. Moving largely by sheet flow, this area only exhibits enhanced flow as it merges with the ice stream between the 1500- and 1000-m surface elevation contours. An additional 22% of the basin is drained by the fast moving tributary that merges with the ice stream just before it enters the fjords of Zachariæ Isstrøm and Nioghalvfjerdsfjorden. This tributary develops distinct ice-stream-like shear margins and fast flow just upstream of the subglacial basin that lies beneath the ice plain. A more detailed exploration of these ice dynamics associated with this basin and plain is described in section 4.

3. Mass Balance

Basin-wide mass balance can be established by measuring the flux at gates near grounding lines and comparing it with the estimated flux from accumulation data and ablation models [*Rignot et al.*, this issue, 1997]. *Rignot et al.* [2001] have examined the mass balance of Zachariæ Isstrøm and Nioghalvfjerdsfjorden in this manner and determined a slightly negative mass balance. Here we take advantage of the additional flux gates along the length of the ice stream to estimate variations in local mass balance.

In deriving the velocity map in Plate 1 we solved for the interferometric baselines with balance velocities as a source of control. We were careful to select only slow moving points outside the ice stream, where the absolute errors are small. The ice stream speeds at the gates (60–150 m/yr) are significantly larger than the control speeds (1–30 m/yr), so that errors (5 m/yr) are small with respect to the flow speeds. For areas outside the ice stream, however, the fractional errors in velocity are too big to allow assessment of mass balance. In fact, where there is little spatial variation in the sheet flow, the interferometric velocities will capture the trend in the balance velocities, and any measurement in these areas will, by definition, show the ice sheet to be in balance. Thus, in this section we limit our investigation as much as possible to the ice stream itself.

Figure 4 shows several fluxgates determined using subsections of profiles T4–T8. We began with profile T8 and computed flow lines extending upstream from a subsection of the profile that intersected the other profiles not too far outside the border of the ice stream. We used the SRI velocities on the lower part to determine the flow lines. When these flow lines strayed outside the area where we had velocity data, we switched to using the surface slopes from the smoothed DEM to continue the flow lines to the divide. The flow lines and each pair of fluxgates define individual regions, which are shown with shading in Figure 4. With flow lines as lateral boundaries the only flux entering and leaving each region other than accumulation should be through the bounding fluxgates. We assume any errors in the determination of the flow lines is small with respect to other errors.

Table 1 shows the measured output flux at each profile along with the accumulation flux of the indicated upstream area. The errors on the measured flux were determined assuming an ice thickness error of 10 m and the velocity error for the component of velocity normal to the fluxgate. Much of the velocity and thickness error is due to errors that should average out in the integration to compute the flux. Since we had no way of determining the spectral properties of the errors, however, we took a conservative approach and assumed that the errors were all in the form of a uniform error along the profile, so that the errors do not average out. Accumulation fluxes were computed by integrating the PARCA accumulation map (R. C. Bales et al., Accumulation map for the Greenland ice sheet, submitted to *Geophysical Research Letters*, 2001, hereinafter referred to as Bales et al., submitted manuscript, 2001) over the area upstream of each profile. The nominal accuracy of the map is ±10% [*Thomas et al.*, 2000], which is the value we used in determining errors. Local errors may be larger or smaller depending on the proximity to a measured value, but we have no estimate of this variability. Because the ice stream speeds are significantly larger than the surrounding sheet flow, this suggests either sliding or deformation concentrated largely in a layer of significantly warmer ice near the bed. In either case, the sliding or deformation is concentrated near the bed so that the depth-averaged velocity should be similar to the surface velocity. In the absence of a thermodynamic model that includes the ice stream we assume that surface and depth-averaged velocities within the ice stream are the same. As a consequence, we may slightly overestimate the depth-averaged velocity and bias our flux estimates high by a few percent. This error should be small with respect to other errors. Only accumulation is considered since the profiles are all high on the ice sheet where there is little or no ablation.

The results in Table 1 all show accumulation fluxes roughly 1.7 km^3/yr water equivalent (WE) larger than the measured flux, suggesting thickening rates upstream of the fluxgates of roughly 2–3 cm/yr. Roughly the same additional accumulation flux is present at all gates, indicating that any imbalance is taking place in the dark shaded region shown upstream of the gate T4 in Figure 4. This region in the accumulation map is poorly constrained by accumulation measurements (Bales et al., submitted manuscript, 2001), and the errors could be significantly larger than the nominal 10%. While a thickening cannot be ruled out, it is quite likely that much of the difference between the measured and accumulation fluxes (20%) is the result of error in the accumulation map. No such thickening is evident in repeat airborne surveys separated by 5 years [*Krabill et al.*, 2000]. More ice cores are needed before a better determination can be made.

To examine the mass balance at various points along the ice stream, Table 2 shows flux differences between pairs of adjacent gates. The first two differences (T5-T4 and T6-T5) differ insignificantly from zero. The flux difference T7-T6 is strongly negative but is followed by a similarly positive difference between gates T7 and T8. Since the two nearly cancel each other, it is likely that these results indicate an erroneously low flux measurement at gate T7.

The errors on the individual measurements are too large to detect all but a very large imbalance on the ice stream. As stated earlier, the errors at the individual fluxgates are likely overstated, so that, in fact, the results may be better than stated here. A more accurate estimate is obtained by comparing the difference of the first and last gate (T8-T4). This fluxgate difference indicates that the middle section of the ice stream is

in balance to within the error of ±6 cm/yr. This is consistent with the lack of significant change determined by the repeat laser altimeter measurements [*Krabill et al.*, 2000].

4. Ice Stream Dynamics

While interferometry gives us a detailed view of ice flow at the surface, it does not directly reveal the internal dynamical controls that yield an ice stream. Flow depends on conditions within the ice column as well as conditions at the bed. Lacking direct observations at the bed, we use a model inversion constrained by remotely sensed data to investigate the dynamics of the Northeast Greenland Ice Stream. In particular, we use the model to examine the basal shear stress beneath the ice stream.

Ice flow takes place by some combination of three processes: internal deformation of the ice, sliding over the bed, and deformation of a weak bed (both in the strictest sense and in the broadest sense [*Engelhardt and Kamb*, 1998]). Inland ice frozen to the bed (as is likely the case for much of the slow moving ice in Plate 1) moves entirely by internal deformation. Large driving stresses and rapid motion often indicate sliding over a bed strong enough to support the ice. This is the dominant source of motion for many outlet glaciers in Greenland and Antarctica. Flow due to a deforming bed (e.g., the Ross Ice Streams, West Antarctica) is dynamically similar to ice shelf flow with rapid motion in the presence of low driving stresses [*MacAyeal*, 1989]. Observations of this type of flow indicate significant temporal variability in flow rates can occur. For example, there is currently a large negative mass imbalance for Ice Stream B [*Shabtaie and Bentley*, 1987; *Whillans and Bindschadler*, 1988], and flow stopped over much of Ice Stream C ~140 years ago [*Retzlaff and Bentley*, 1993]. A determination of which mode of flow predominates is central to our understanding of the nature of the fast flow in the Northeast Greenland Ice Stream.

4.1. Model and Inverse Methods

Our results are based on a finite element model of ice stream flow that was developed for applications to West Antarctic ice streams. This model is described by *MacAyeal* [1989], and its application to West Antarctic ice streams is described by *Hulbe and MacAyeal* [1999]. In brief, the model determines the velocity and stress fields as functions of ice thickness, surface elevation, a basal drag coefficient (the basal drag vector is determined by the model), and various boundary conditions, including the location of seaward ice fronts, ice shelf grounding lines, and connections with nonstreaming inland ice sheet. A full description of the model and its approximations is given by *MacAyeal* [1989]. The model is most applicable when the ice flow is dominated by basal motion.

We inverted the forward model to find the model parameters (e.g., basal shear stress) that minimized the misfit between a model-derived velocity field and its observed counterpart. This inversion relied on "adjoint trajectory methods" [*MacAyeal*, 1989; *Rommelaere and MacAyeal*, 1997], which are related to optimal control theory. With this method an adjoint trajectory version of the model is created (many model equations are "self-adjoint," and thus little modification of the forward model code is needed to solve inverse problems) to develop automatic and objective means to evaluate the "cost functions" (i.e., least squares misfits between model fields and observed fields) as it varies with changes in undetermined parameters. Similar methods have been used successfully to study the basal friction field of Ice Stream E, Antarctica, where the velocity data were derived using feature-tracking methods [*MacAyeal et al.*, 1995].

The flow law rate constant of ice, B, varies strongly with temperature [*Paterson*, 1994]. Cold ice deforms at a slower rate than warmer ice and is thus capable of supporting more shear stress at the margins. As a result, an assumption of colder ice in the inversion will lead to lower estimated basal shear stresses as more of the resistive stress is attributed to side drag at the margins. Conversely, an assumption of warmer ice leads to larger basal shear stress estimates.

We do not have an accurately modeled temperature field for the ice stream. Instead, we examined the sensitivity of the inversions to temperature by using "cold" and "warm" models that roughly bracket the expected range of temperatures. For the cold model we used the Greenland Ice Sheet Project (GISP 2) profile increased by 6°, which brings the profile near to the pressure melting point at the bed. This somewhat arbitrary adjustment yields a temperature profile, which, with the possible exception of the extreme upper regions of the ice stream, is colder than expected. The ice stream model uses a vertically integrated value for the flow law constant, B, which for the cold model yields $B = 2.0 \times 10^5$ s$^{1/3}$ kPa. The warm model assumes a simple linear profile from the approximate mean annual temperature over the ice plain of −20° to −2°C at the bed. Essentially, the linear profile neglects the effects of advection, resulting in a temperature profile that should be warmer than actual temperatures for the entire ice stream. This yields a vertically averaged value for the flow law constant of $B = 1.25 \times 10^5$ s$^{1/3}$ kPa. In both models the flow law exponent was set to $n = 3$.

Strain softening of the ice [*Budd and Jacka*, 1989] can also weaken the ice at the margins and consequently can affect the basal shear stress. To examine the magnitude of this effect, we also inverted a "soft" model, where B was reduced by a factor of 5 ($B = 5.0 \times 10^4$ s$^{1/3}$ kPa) along the margins and the flow parameters from the cold model used elsewhere.

In performing the inversions, all input data (e.g., velocity and surface and bed topography) were interpolated to the nodes of the finite element mesh. We used the bed data shown in Figure 3 and a satellite altimetry–derived elevation model (Bamber et al., submitted manuscript, 2001), which had similar resolution to that of the finite element mesh. The "resolution" of this mesh varies from ~3 to 8 km. Coarser resolution was used in slow moving regions, and finer resolution was used in the faster moving areas. The results were all reinterpolated to a regular grid for plotting (Plate 3). As a result, the computed values (e.g., driving stress) effectively have been smoothed by the variable resolution of the finite element mesh.

4.2. Inversion Results

The driving stress (proportional to slope times thickness) is shown in Plate 3. In the upper narrow region of the ice stream the driving stresses are in the range of 30–40 kPa. As the ice stream widens out, the driving stress increases to 50–70 kPa over the next several hundred kilometers. Just upstream of the ice plain, there is a band of increased driving stress with peaks as high as 100 kPa. Over the ice plain, driving stresses decrease to 10–40 kPa. A peak in driving stress followed by a rapid decline associated with a large increase in flow speed is characteristic of the streaming onsets of the Ross Ice Streams [*Bindschadler et al.*, 2001]. Unlike the case in West Antarctica, where driving stresses continue to decline all the way to the grounding line, the driving stress increases on the other side of

the ice plain to roughly 150 kPa just above the grounding line. On the floating ice tongue of Nioghalvfjerdsfjorden (not shown) the driving stress drops to nearly zero.

The fast flow despite the decrease in driving stresses suggests that the bed is much weaker under the ice plain. To investigate further, we have inverted both the warm and cold finite element models constrained by the velocity and topography observations. Plate 3b shows the measured flow speed, and the resulting speed for the cold model fit is shown in Plate 3c. The overall misfit in speed is just over 5 m/yr for both the cold and warm models. The model fit had the most difficulty in capturing some of the subtle details in the narrow upstream region of the ice stream. In this area of slower moving ice the absolute errors are small, so their overall contribution to the cost function used in the inversion is small relative to the faster moving areas with larger errors. As a consequence, the inversion algorithm focuses more on improving the fit in the faster moving downstream areas.

Plate 3d shows the inferred basal shear stress for the cold model. In general, it shows a pattern of highs and lows similar to that of the driving stress, indicating that the basal shear stress supports most of the driving stress over much of the ice stream. To better compare the basal and driving stresses, we computed the ratios of the basal to driving stress for both the cold (Plate 3e) and warm (Plate 3f) models. Plates 3e and 3f reveal an area on the ice plain where the basal shear stress is significantly lower than the driving stress. The average driving stress under the ice plain for the main branch of the ice stream (e.g., the dark blue area in Plate 3d) is 23 kPa, while the average basal shear stresses are 14 and 15 kPa for the cold and warm models, respectively. Over much of this area (e.g., the green areas in Plate 3d) the basal shear stress supports just over 50% of the driving stress. We also analyzed the data on the basis of the force budget approach [*Van der Veen*, 1999]. The results suggest that most of the remaining driving stress is taken up by side drag at the margins. We also inverted the soft model (not shown), which yielded basal shear stresses under the ice plain that were only slightly raised with respect to the cold model (<2 kPa).

Our results suggest that the bed beneath the ice plain is weak and a significant portion of this area can support only 10–15 kPa. Similar results hold for the smaller area under the tributary that merges with the ice stream just upstream of Nioghalvfjerdsfjorden. These low basal shear stresses are well within the range where the model for streaming flow is appropriate and suggest that the fast motion in this region is due to flow over a weak bed. There were only marginal differences between the cold, warm, and soft models, suggesting that the conclusion of a deforming bed is robust with respect to temperature and strain softening. While there are results that suggest polythermal ice (a basal layer of temperate ice tens to hundreds of meters thick) in this region [*Greve*, 1997], the driving stresses over the ice plain are too weak to cause significant deformation flow, even if there is a relatively thick layer of temperate basal ice. Thus the significant departure of the ice plain from a typical ice sheet geometry is likely the result of a weak bed. This may be due to the accumulation of sediment in the closed basin and to the effects of the basin on drainage and resulting low effective water pressure. The inferred basal shear stresses, however, suggest that the bed is significantly stronger (10–15 kPa) than in some areas of West Antarctica (2 kPa) [*Kamb*, 1991]. This could be the result of a variety of causes including differences in the till, a greater preponderance of sticky spots [*Alley*, 1993], or differences in the subglacial drainage.

The basal shear stress along the middle portion of the ice stream exhibits a pattern of highs and lows similar to the driving stress but with slightly reduced magnitudes (i.e., ~70–80% of the driving stress). The magnitudes of the inferred basal shear stresses in this region are beyond the range where the model is applicable. Analysis of the model indicates that when there is substantial deformation due to vertical shear, the model correctly predicts the locations of "sticky spots" but tends to underestimate the basal shear stress. Further development of the model to include the effect of vertical shear is needed to enable quantitatively meaningful estimates of the shear stress at the bed. Qualitatively, the results indicate that the bed is capable of supporting most or all of the driving stress and that there are variations in the basal shear stress that correspond roughly with those in the driving stress. Given the rough nature of the bed (see Figures 2 and 3), these fluctuations likely are tied to peaks and valleys in the bedrock topography. Here the presence of polythermal ice, as suggested by *Greve* [1997], could have a significant effect on the flow. With speeds of 50–100 m/yr the motion over the central region of the ice stream could result from deformation of a basal layer of warm ice, sliding over a strong bed, or some combination of these processes.

The results shown in Plates 3e and 3f suggest that basal shear stress is significantly lower than driving stress in the narrow upstream region where enhanced flow is first visible in the ice stream. The inversion over the whole ice stream missed subtle details of the flow field in the upstream region, so we performed separate inversions that included just the upstream area. This yielded improved results, with model data speed misfits of <1.5 m/yr. The basal shear stresses inferred from these inversions, however, did not differ significantly from those shown in Plate 3, so they are not shown here. The basal shear stress along a 53-km section of this region averaged 24 kPa with the cold model, while the corresponding driving stress was 42 kPa. This suggests that the geometry of this narrow region of the ice stream may be due to a localized weakening of the bed. The width of the ice stream is sufficiently narrow that side drag can take up much of the driving stress, allowing moderate driving stresses (e.g., 40–50 kPa) over a potentially weak bed (10–25 kPa). Further investigation of the dynamics of this region is described by *Fahnestock et al.* [this issue].

5. Summary

We have presented several new remotely sensed data sets for the Northeast Greenland Ice Stream. In particular, the recently discovered Northeast Greenland Ice Stream is now one of the most completely mapped ice streams in terms of its velocity field. With the interferometric SAR velocity data and the new bed topography [*Bamber et al.*, this issue], we have been able to establish that the ice stream has a channel over part of its length. The channel extent is not sufficient, however, to entirely explain the linear geometry of the ice stream. The bed topography appears to play a role in the initiation of the ice stream by forcing an area of strongly converging ice flow deep within the interior of the ice sheet. With the addition of the PARCA accumulation map (Bales et al., submitted manuscript, 2001), we have been able to establish that the ice stream is in, or close to within, balance, which is consistent with observations from repeat laser profiles [*Krabill et al.*, 2000].

Inversions of an ice stream model constrained by the velocity and bed data suggest that a weak bed yields an ice plain upstream of Zachariæ Isstrøm and Nioghalvfjerdsfjorden, leading to streaming flow similar to that of West Antarctic ice streams. The presence of a weak bed has implications for the stability of the region. If it is a weak plastic bed, such as has been suggested for West Antarctic ice streams [*Tulaczyk et al.*, 2000], then it may be subject to a delicate thermodynamic balance that could potentially lead to a shutdown, as on Ice Stream C. This may be unlikely, though, as ice sheet models predict relatively warm temperature profiles and polythermal ice in this region [*Greve*, 1997]. While the model used in our inversions does not strictly apply over the several hundred kilometers along the central length of the ice stream, it does indicate that the bed is much stronger in this region. As a result, this central region of the ice stream could act as a stabilizing influence to limit inland retreat in the event of any large increase in speed over the weak-bedded portion of the ice stream. Finally, the model indicates that the bed may be weak in the upstream reaches of the ice stream, which is discussed further by *Fahnestock et al.* [this issue].

Acknowledgments. I. Joughin performed his contribution to this work at the Jet Propulsion Laboratory, California Institute of Technology, under contract with NASA. M. Fahnestock and S. Gogineni were funded by NASA Polar Programs. J. Bamber's contribution was funded by NERC grant GR3/9791. We thank W. Krabill of NASA/Wallops for the laser altimeter data, R. Thomas for the GPS data, and R. Bales, J. R. McConnell, E. Mosley-Thompson, and B. Csthao for the accumulation map. We acknowledge the help of Dilip Tammana, Kuok-Wai Wong, Kok Lin Tee, and Yeh-Chiing Wong in processing the radar depth sounder data. Many discussions with Eric Rignot also contributed to this paper. Finally, we thank the three anonymous reviewers whose comments added greatly to this paper.

References

Alley, R. B., In search of ice-stream sticky spots, *J. Glaciol.*, *39*(133), 447–454, 1993.

Bamber, J. L., S. Ekholm, and W. B. Krabill, A new, high-resolution digital elevation model of Greenland fully validated with airborne laser altimeter data, *J. Geophys. Res.*, *106*, 6733–6745, 2001.

Bamber, J. L., R. Layberry, and S. P. Gogenini, A new ice thickness and bed data set for the Greenland ice sheet, 1, Measurement, data reduction, and errors, *J. Geophys. Res.*, this issue.

Bales, R. C., J. R. McConnell, and E. Mosley-Thompson, Accumulation map for the Greenland ice sheet: 1971–1990, *Geophys. Res. Lett.*, *28*(15), 2967–2970, 2001.

Bindschadler, R., J. L. Bamber, and S. Anandakrishnan, Onset of streaming flow in West Antarctica, in *West Antarctic Ice Sheet, Antarct. Res. Ser.*, vol. 77, edited by R. Alley and R. M. Bindschadler, pp. 123–136, AGU, Washington, D. C., 2001.

Budd, W. F., and T. H. Jacka, A review of ice rheology for ice sheet modelling, *Cold Reg. Sci. Technol.*, *16*, 107–144, 1989.

Ekholm, S., A full-coverage, high-resolution, topographic model of Greenland, computed from a variety of digital elevation data, *J. Geophys. Res.*, *101*(B10), 21,961–21,972, 1996.

Engelhardt, H., and B. Kamb, Basal sliding of Ice Stream B, West Antarctica, *J. Glaciol.*, *44*(147), 223–230, 1998.

Fahnestock, M., R. Bindschadler, R. Kwok, and K. Jezek, Greenland ice sheet surface properties and ice dynamics from ERS-1 SAR imagery, *Science*, *262*, 1530–1534, 1993.

Fahnestock, M., I. Joughin, T. A. Scambos, R. Kwok, W. B. Krabill, and S. Gogineni, Ice-stream-related patterns of ice flow in the interior of northeast Greenland, *J. Geophys. Res.*, this issue.

Gogineni, S., D. Tammana, D. Braaten, C. Leuschen, T. Akins, J. Legarsky, P. Kanagaratnam, J. Stiles, C. Allen, and K. Jezek, Coherent radar ice thickness measurements over the Greenland ice sheet, *J. Geophys. Res.*, this issue.

Goldstein, R. M., H. Engelhardt, B. Kamb, and R. M. Frolich, Satellite radar interferometry for monitoring ice sheet motion: Application to an Antarctic ice stream, *Science*, *262*, 1525–1530, 1993.

Gray, A. L., K. E. Mattar, and P. W. Vachon, InSAR results from the RADARSAT Antarctic mapping mission data: Estimation of glacier motion using a simple registration procedure, paper presented at IEEE Geoscience and Remote Sensing Symposium '98, Seattle, Wash., 1998.

Greve, R., Application of a polythermal three-dimensional ice sheet model to the Greenland ice sheet: Response to steady-state and transient climate scenarios, *J. Clim.*, *10*(5), 901–918, 1997.

Hulbe, C. L., and D. R. MacAyeal, A new thermodynamical numerical model of coupled ice sheet, ice stream, and ice shelf flow, *J. Geophys. Res.*, *104*(B11), 25,349–25,366, 1999.

Joughin, I., M. Fahnestock, S. Ekholm, and R. Kwok, Balance velocities for the Greenland ice sheet, *Geophys. Res. Lett.*, *24*(23), 3045–3048, 1997.

Joughin, I., R. Kwok, and M. Fahnestock, Interferometric estimation of three-dimensional ice-flow using ascending and descending passes, *IEEE Trans. Geosci. Remote Sens.*, *36*(1), 25–37, 1998.

Joughin, I., L. Gray, R. Bindschadler, S. Price, D. Morse, C. Hulbe, K. Mattar, and C. Werner, Tributaries of West Antarctic ice streams revealed by RADARSAT interferometry, *Science*, *286*, 283–286, 1999.

Joughin, I. R., M. Fahnestock, and J. Bamber, Ice flow in the Northeast Greenland Ice Stream, *Ann. Glaciol.*, *31*, 141–146, 2000.

Kamb, B., Rheological nonlinearity and flow instability in the deforming bed mechanism of ice stream motion, *J. Geophys. Res.*, *96*(B10), 16,585–16,595, 1991.

Krabill, W., W. Abdalati, E. Frederick, S. Manizade, C. Martin, J. Sonntag, R. Swift, R. Thomas, W. Wright, and J. Yungel, Greenland ice sheet: High-elevation balance and peripheral thinning, *Science*, *289*, 428–430, 2000.

MacAyeal, D. R., Large-scale ice flow over a viscous basal sediment: Theory and application to Ice Stream B, Antarctica, *J. Geophys. Res.*, *94*(B4), 4071–4088, 1989.

MacAyeal, D., R. Bindschadler, and T. Scambos, Basal friction of Ice Stream E, West Antarctica, *J. Glaciol.*, *41*(138), 247–262, 1995.

Michel, R., and E. Rignot, Flow of Glacier Moreno, Argentina, from repeat-pass shuttle imaging radar images: Comparison of the phase correlation method with radar interferometry, *J. Glaciol.*, *45*(149), 93–102, 1999.

Mohr, J. J., N. Reeh, and S. N. Madsen, Three-dimensional glacial flow and surface elevation measured with radar interferometry, *Nature*, *391*(6664), 273–276, 1998.

Paterson, W. S. B., *The Physics of Glaciers*, 3rd ed., 480 pp., Pergamon, New York, 1994.

Reeh, N., C. E. Bøggild, and H. Oerter, Surge of Storstrømmen, a large outlet glacier from the inland ice of North-East Greenland, *Rapp. Grønl. Geol. Unders.*, *162*, 201–209, 1994.

Retzlaff, R., and C. R. Bentley, Timing of stagnation of Ice Stream-C, West Antarctica, from short-pulse radar studies of buried surface crevasses, *J. Glaciol.*, *39*(133), 553, 1993.

Rignot, E. J., S. P. Gogineni, W. B. Krabill, and S. Ekholm, North and northeast Greenland ice discharge from satellite radar interferometry, *Science*, *276*, 934–937, 1997.

Rignot, E., G. Buscarlet, B. Csatho, S. Gogineni, W. Krabill, and M. Schmeltz, Mass balance of the northeast sector of the Greenland ice sheet: A remote sensing perspective, *J. Glaciol.*, *46*(153), 265–273, 2001.

Rignot, E., S. P. Gogenini, I. Joughin, and W. B. Krabill, Contribution to the glaciology of northern Greenland from satellite radar interferometry, *J. Geophys. Res.*, this issue.

Rommelaere, V., and D. R. MacAyeal, Large-scale rheology of the Ross Ice Shelf, Antarctica, computed by a control method, *Ann. Glaciol.*, *24*, 43–48, 1997.

Shabtaie, S., and C. R. Bentley, West Antarctic ice streams draining into the Ross Ice Shelf: Configuration and mass balance, *J. Geophys. Res.*, *92*(B2), 1311–1336, 1987.

Thomas, R. H., B. M. Csatho, S. Gogineni, K. C. Jezek, and K. Kuivinen, Thickening of the western part of the Greenland ice sheet, *J. Glaciol.*, *44*(148), 653–658, 1998.

Thomas, R. H., T. Akins, B. Csatho, M. Fahnestock, S. Gogineni, C. Kim, and J. Sonntag, Mass balance of the Greenland ice sheet at high elevations, *Science*, *289*, 426–428, 2000.

Tulaczyk, S., W. B. Kamb, and H. F. Engelhardt, Basal mechanics of

Ice Stream B, West Antarctica, 2, Undrained plastic bed model, *J. Geophys. Res.*, *105*(B1), 483–494, 2000.

Van der Veen, C. J., *Fundamentals of Glacier Dynamics*, 462 pp., A.A. Balkema, Brookfield, Vt., 1999.

Whillans, I. M., and R. A. Bindschadler, Mass balance of Ice Stream B, West Antarctica, *Ann. Glaciol.*, *11*, 187–193, 1988.

J. L. Bamber, Centre for Remote Sensing, School of Geographical Sciences, University of Bristol, University Road, Bristol BS8 1SS, England, UK. (j.l.bamber@bristol.ac.uk)

M. Fahnestock, Earth System Science Interdisciplinary Center, University of Maryland, College Park, MD 20740. (mark@essic.umd.edu)

P. Gogineni, Radar Systems and Remote Sensing Laboratory, University of Kansas, Lawrence, KS 66045.

I. Joughin, Jet Propulsion Laboratory, California Institute of Technology, MS 300-235, 4800 Oak Grove Drive, Pasadena, CA 91109. (ian@rgps1.jpl.nasa.gov)

D. MacAyeal, Department of Geophysical Sciences, University of Chicago, 5734 South Ellis Avenue, Chicago, IL 60637. (drm7@midway.uchicago.edu)

(Received August 3, 2000; revised January 2, 2001;
accepted January 19, 2001.)